Least-Squares Low-Frequency Extrapolation for Full-Waveform Inversion Without Cycle Skipping

Israel Owolabi[1], Rehman Ali[2], Trevor Mitcham[2], Victoria Nketia[1], Melanie Singh[3], and Nebojsa Duric[123]

[1]Department of Electrical and Computer Engineering, University of Rochester, Rochester, New York 14642, USA
[2]Department of Imaging Sciences, University of Rochester, Rochester, New York 14642, USA
[3]Department of Biomedical Engineering, University of Rochester, Rochester, New York 14642 USA

ABSTRACT

In most ultrasound transducer designs, priority is given to a high frequency operation to maximize spatial resolution in conventional B-mode reflectivity imaging. However, applying full-waveform inversion (FWI) with the same high frequency hardware presents significant challenges, most notably the risk of cycle skipping artifacts. These artifacts arise when a phase mismatch between the predicted and measured wavefields leads the inversion to converge to incorrect solutions (false local minimal). Overcoming this issue requires the presence of low frequency content, which improves the robustness of the inversion by increasing the wavelength of the waveform and thereby enables better alignment between the predicted and measured wavefields. Least-squares extrapolation of low frequency data provides the FWI with a good initial model for reconstruction of tissue parameters and builds upon our previous work on frequency-differencing to circumvent cycle-skipping artifacts in UST sound speed image reconstruction.

Keywords: Ultrasound tomography, nonlinear inverse problems, waveform inversion, cycle-skipping

1. INTRODUCTION

Ultrasound tomography (UST) is an advanced imaging technique that uses the transmission of ultrasound waves through tissue to quantitatively reconstruct multiple acoustic properties, such as sound speed, density, and attenuation.[1–4] In multi-frequency inversion, the measured data are processed sequentially, starting with the inversion of the lowest available frequency components and gradually introducing higher frequency information.[5,6] The limited availability of low frequency signals in most ultrasound transducers optimized for B-mode imaging poses a significant barrier to the broader adoption of FWI, which relies on low frequency components (below 1 MHz) to mitigate cycle skipping artifacts. This challenge arises from inaccuracies in the initial model.[7] This occurs because FWI minimizes the difference between the simulated and measured signals. When the simulated signal is shifted, delayed, or advanced by more than half a cycle relative to the measured signal, the model updates in the wrong direction, a phenomenon known as cycle skipping. Incorporating low-frequency data improves the robustness of FWI by extending the half-cycle window, enabling the algorithm to overcome errors in the starting model.[5,8]

However, low frequency ultrasound information is challenging to extract when the system exhibits limited sensitivity below a known operational band of the transducer. In this work, we propose a frequency-domain autoregressive model to synthesize low frequency signal components using only data from the available high-fidelity frequency range of any transducer (e.g., 1 - 4 MHz); we employ a regularized least-squares inversion framework to estimate the coefficients that will be used to extrapolate low frequency ultrasound signals from the available high frequency measurements. The method assumes that each low frequency component can be approximated as a

Further author information: (Send correspondence to Israel Owolabi)
Israel Owolabi: E-mail: iowolabi@ur.rochester.edu

Medical Imaging 2026: Ultrasonic Imaging and Tomography, edited by Christian Boehm, Mohammad Mehrmohammadi, Shawn Liangzhong Xiang, Proc. of SPIE Vol. 13931, 139310I · 2026 Published by SPIE
1605-7422 · doi: 10.1117/12.3084570

linear combination of higher frequency components. The optimal set of regression coefficients for each transmit-receive pair was estimated by solving a regularized inverse problem that minimizes the discrepancy between the predicted and known low frequency data in FWI. This approach avoids reliance on noise-prone frequency band measured data and enables robust extrapolation into frequency regions that are otherwise inaccessible to the acquisition system. Experimental results on RF data demonstrate the effectiveness of the method in synthesizing low frequency content with high fidelity, offering potential benefits for improving the performance of FWI in reconstructing the acoustic properties of the tissue by minimizing the error between simulated and measured signals after applying the least-squares extrapolated data.

2. BACKGROUND

2.1 Frequency-Domain FWI

The UST reconstruction problem involves estimating the acoustic properties of tissue from pressure wavefields recorded by transducers positioned along the boundary. In the frequency domain, the objective function for full-waveform inversion (FWI) is formulated as the sum of squared differences between the measured and predicted signals, expressed as follows:

$$E(\omega, \mathbf{s}) = \frac{1}{2} \sum_{i=1}^{N} \left\| \mathbf{p_i}(\omega, \mathbf{s}) - \mathbf{p_{obs,i}}(\omega) \right\|_2^2 . \tag{1}$$

where $\mathbf{p_i}$ and $\mathbf{p_{obs,i}}$ are the simulated and observed pressure measurements on the ring array for the $\mathbf{i^{th}}$ single-element transmission ($\mathbf{i}$ ranges from 1 to N, the number of elements on the ring array). Using finite difference methods,[9] we solve the 2D Helmholtz equation to obtain a pressure field $\mathbf{u}$ for a given source δ, frequency $\omega = 2\pi f$, and slowness $\mathbf{s}$ (i.e, the reciprocal of sound speed):

$$(\nabla^2 + \omega^2 \mathbf{s}^2)\mathbf{u}(\omega, \mathbf{s}) = \delta(\omega), \tag{2}$$

See prior work[10] for details on the complete implementation of frequency-domain FWI.

3. INNOVATION

A least-squares approach was used to extrapolate low frequency data from a known high-fidelity frequency band (e.g., 1-4 MHz). Let $f_i \in [1.0, 2.0]$ MHz be the set of low frequencies that are known to have high fidelity signals, and $\Delta f_j \in [0.20, 1.0]$ MHz be the set of frequency shifts with step size of 0.05 MHz and 0.01 MHz, respectively. For each desired frequency f_i, we generate shifted frequencies f_{ij}:

$$f_{ij} = f_i + \Delta f_j \qquad \text{for} \quad j = 1, ..., J. \tag{3}$$

We computed the discrete-time Fourier transform (DTFT) of the RF data at all shifted frequencies (3), resulting in the synthesis matrix of $\mathbf{G}$, which represents the sets of known signals at higher frequencies f_{ij}. The observed data $\vec{d}$ at low frequency f_i was extracted directly by applying the Fourier transform to the RF signals at f_i. We model the low-frequency components of the signal $d_i := d(f_i)$ (single entry of $\vec{d}$) as a linear combination of shifted high frequency components from the same dataset. The mapping coefficients $\vec{\alpha}$, estimated from the available high-frequency measurements, are used to relate the high-frequency band to the target low-frequency band. This relationship is expressed as:

$$d_i := d(f_i) \approx \sum_{j=1}^{J} \alpha_j \, d(f_{ij}) := \mathbf{G}_i \vec{\alpha}. \tag{4}$$

where $d_i = d[f_i]$ are the entries of $\vec{d}$, $G_{ij} = d[f_i + \Delta f_j]$ are the entries of $\mathbf{G}$, $\alpha_j = \alpha[\Delta f_j]$ are the entries of $\vec{\alpha}$, and $\mathbf{G}_i$ refers to a single row of the full $\mathbf{G}$ matrix. Stacking all frequency samples into vectors, the model can be written in matrix form as:

$$\vec{d} = \begin{bmatrix} d[f_1] \\ d[f_2] \\ \vdots \\ d[f_I] \end{bmatrix} = \begin{bmatrix} d[f_1+\Delta f_1] & d[f_1+\Delta f_2] & \cdots & d[f_1+\Delta f_J] \\ d[f_2+\Delta f_1] & d[f_2+\Delta f_2] & \cdots & d[f_2+\Delta f_J] \\ \vdots & \vdots & \ddots & \vdots \\ d[f_I+\Delta f_1] & d[f_I+\Delta f_2] & \cdots & d[f_I+\Delta f_J] \end{bmatrix} \begin{bmatrix} \alpha[\Delta f_1] \\ \alpha[\Delta f_2] \\ \vdots \\ \alpha[\Delta f_J] \end{bmatrix} = \mathbf{G}\vec{\alpha}. \tag{5}$$

The coefficients α_j are obtained by solving a Tikhonov-regularized least-squares problem using overlapping frequency bands:

$$\vec{\alpha}^{LS} = \underset{\vec{\alpha}}{\operatorname{argmin}} \left(\|\mathbf{G}\vec{\alpha} - \vec{d}\|_2^2 + \lambda \|\vec{\alpha}\|_2^2 \right) \tag{6}$$

Here (6), λ is a small regularization parameter to ensure numerical stability in the presence of noise or poorly conditioned matrices. Once the synthesis coefficients $\vec{\alpha}$ are computed for each transmit-receive pair, they are applied to the high-frequency data to recover the complete set of known low frequency measurements:

$$\hat{d}_i = \mathbf{G}_i \vec{\alpha}^{LS} \tag{7}$$

The recovered data $\hat{d}_i$ was then compared with the original ground-truth (4) to validate the precision of the synthesis. Finally, to extrapolate into frequency regions where no measured data exists originally exists (e.g. $f_{low} \in [0.15, 0.35]$) MHz, we applied the previously learned coefficients $\vec{\alpha}$ to a newly constructed matrix of frequency-shifted spectra yielding synthesized spectra at f_{low}:

$$\hat{d}(f_{\text{low}}) = \sum_{j=1}^{J} \alpha_j^{LS}\, d(f_{\text{low}} + \Delta f_j) \tag{8}$$

4. METHODS

4.1 Starting Model Based on Least-Square Low Frequency Extrapolation

Frequency-domain full waveform inversion (FWI) is commonly performed from the lowest available frequency to the highest to mitigate cycle skipping and achieve high-resolution reconstructions. However, the absence of sufficiently low-frequency components in the recorded data often limits the ability of FWI to recover large-scale structures, thus requiring accurate starting models. To address this limitation, we propose a least-squares frequency synthesis approach that reconstructs missing low-frequency data directly from the available higher frequencies. The method formulates an inverse problem in which the unknown low-frequency components are expressed as a linear combination of neighboring high-frequency signals, with the combination weights estimated through a regularized least-squares solution. This approach enables the generation of physically consistent low-frequency information without requiring additional data acquisition. The synthesized low-frequency data were then used as a starting model for FWI, allowing the inversion to begin at higher frequencies while maintaining cycle-skipping robustness. The resulting reconstructions are compared against those obtained from homogeneous starting models under identical conditions.

4.2 Breast Imaging

I) In silico Breast Imaging: We use the k-Wave simulation toolbox[11] to simulate the channel data received from an 11 cm diameter ring array with a 2.5 MHz center frequency transmit pulse (75% fractional bandwidth) from each of the 256 elements. A numerical phantom based on the MATLAB built-in modified Shepp–Logan phantom was used to construct the sound speed and attenuation maps used in the simulation. No Noise was added to the simulated data. A starting homogeneous model of 1515 m/s was used for both both FWI and the least-squares-FWI method (LS-FWI) described in Section 4.1, using frequencies ranging from 0.60 to 1.25 MHz and the Least-squares extrapolated signal from 0.15 to 0.6 MHz for the reconstruction of the sound speed image. The convergence was evaluated by calculating the root mean square (RMS) error between the two results.

II) In vivo Breast Imaging: We proceed to use raw ultrasound channel data from a whole-breast ultrasound tomography system (Delphinus Medical Technologies Inc., Novi, MI) to reconstruct the speed of sound in the breast. Here, FWI was applied from 0.45 to 1.25 MHz, and based on the least-squares extrapolated data from 0.15 to 0.45 MHz, FWI reconstructs the breast sound speed profile from a homogeneous starting model of 1480 m/s.

4.3 Experimental Transcranial Imaging

First, an intact human skull sample was sourced through Skulls Unlimited International, Inc. (Oklahoma City, OK), and subsequently degassed under vacuum for 24 hours in distilled water. Then a tissue-mimicking gelatin phantom with three high sound speed targets (gelatin mixed with 20% alcohol; 1620 m/s) was inserted into the degassed skull for data collection. A Verasonics Vantage NXT 256 ultrasound system was paired with an 11 cm diameter ring transducer with a 1.5 MHz center frequency and 256 elements to collect the experimental data with a 1.5 MHz transmit frequency. In this experiment, each reconstruction began with a 1600 m/s homogeneous model. The regular FWI used several frequency pairs whose values ranged from 0.35 to 0.50 MHz and the low-frequency data (0.20 to 0.35 MHz) extrapolated by least-squares followed by FWI from 0.35 to 0.50 MHz and compared the results to the CT ground truth image.

5. RESULTS AND DISCUSSION

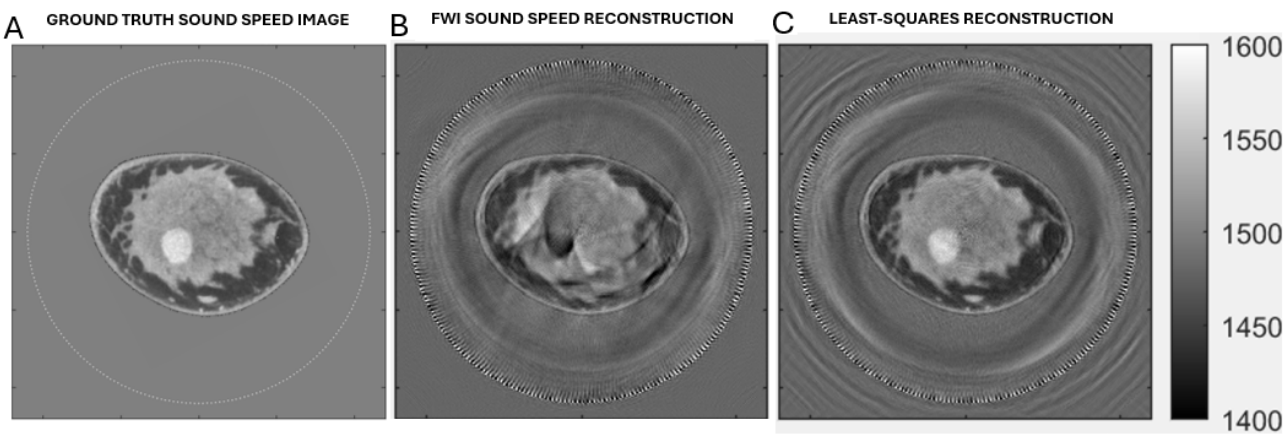

Figure 1. Impact of Regularized Least-Squares Low-Frequency Extrapolation on FWI in a Breast Imaging Simulation. A) Ground-truth image, B) FWI image from 0.6 to 1.25 MHz, and C) FWI image based on low-frequency data (0.15 to 0.6 MHz) extrapolated by regularized least squares followed by FWI from 0.6 to 1.25 MHz. The extrapolated low-frequency data helps FWI avoid cycle skipping.

Figure 1 (A) Ground-truth sound-speed distribution used in the k-Wave simulations. (B) Sound-speed reconstruction obtained by applying frequency-domain FWI to the raw received-channel data. (C) Sound-speed reconstruction obtained when FWI is initialized with low-frequency content synthesized by the proposed regularized least-squares extrapolation method. The least-squares (LS) frequency extrapolation method produces physically consistent synthetic low-frequency components that help stabilize the inversion process. By supplying the inversion with coherent low frequencies that are otherwise absent in the measured data, the LS approach effectively mitigates cycle skipping, improves convergence, and enhances the recovery of both the high sound-speed inclusions and their surrounding boundary structures. Quantitatively, this improvement is reflected in a substantial reduction in reconstruction error: the root-mean-square (RMS) error in estimated sound speed is 20.6 m/s using conventional FWI, compared to 10.8 m/s when incorporating LS-extrapolated low-frequency data. This shows that the LS method significantly strengthens the stability of the inversion.

Figure 2 shows the waveform inversion on real breast and skull data acquired with a ring-array transducer, comparing reconstructions with and without extrapolated least-squares data. These results demonstrate the

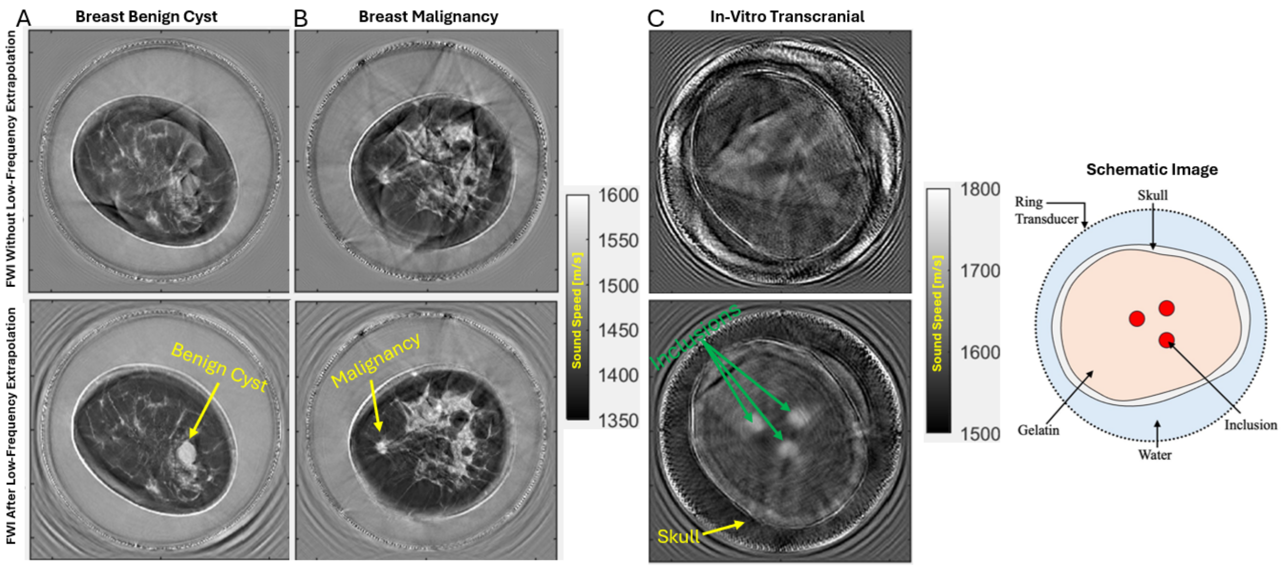

Figure 2. Improving FWI Performance Using Regularized Least-Squares Low-Frequency Extrapolation on real breast and skull with alcohol inclusions data. The top row of A) and B) shows the FWI images of the two breast cases from 0.45 to 1.25 MHz that results in cycle skipping artifacts, and A) and B) (bottom) FWI images of the breast based on extrapolated low-frequency data (0.15 to 0.45MHz) by regularized least squares and updated with data from 0.45 to 1.25 MHz C) (top) is the FWI image of the skull with three inclusions from 0.35 to 0.55MHz, and C) (bottom) is the FWI image from 0.35 to 0.55MHz after reconstruction based on low-frequency data (0.15 to 0.35MHz) extrapolated by regularized least-squares approach. In all cases FWI avoid cycle skipping with the help of the extrapolated low-frequency data.

impact of the least-squares extrapolation approach when used as a starting model for FWI in both breast and transcranial experiments. In Figures 2A and 2B (bottom), reconstructing extrapolated data from 0.15 to 0.45 MHz and updating with 0.45 to 1.25 MHz FWI captures detailed tissue structure and a lesion that was missed due to cycle skipping when using only high-frequency data. These artifacts arise from the use of high-frequency data ranging from 0.45 to 1.25 MHz, in which FWI fails to compensate for the large discrepancies introduced by the 1480 m/s homogeneous starting model. Figure 2C illustrates the inherent difficulty in transmitting high-frequency ultrasound waves through high-impedance structures such as the skull. At these frequencies, bone introduces severe attenuation, scattering, and refractive phase distortions, all of which significantly degrade the fidelity of the recorded wavefield. As a result, the back-propagated wavefields contain insufficient coherent low-frequency energy, making it challenging to accurately reconstruct the underlying brain parenchyma. 2C (bottom) presents the reconstruction obtained using low-frequency data (0.20–0.35 MHz) synthesized using the least-squares (LS) extrapolation method, followed by an update using measurements recorded at 0.35 to 0.50 MHz for transcranial imaging. This combined strategy improves the illumination of deeper structures and stabilizes the inversion in the presence of skull-induced distortions. The resulting image successfully recovers the three internal inclusions, yielding a sound-speed estimate of 1671 m/s, and clearly delineates the skull boundaries, demonstrating the effectiveness of low-frequency supplementation based on LS in overcoming transcranial propagation challenges, unlike 2C (top), where FWI using only 0.35 - 0.50 MHz failed due to cycle skipping artifacts introduced by its large discrepancies from the homogeneous starting model of 1600 m/s and corrupts the entire image.

6. CONCLUSIONS

This work presents a linear frequency-domain autoregressive model and inversion framework to synthesize low frequency ultrasound data from the available high frequency measurements using regularized least-squares. By leveraging the linearity of time-delay information in the frequency domain, we demonstrated that high frequency components can be linearly combined to recover the missing low frequency signals needed to overcome cycle skipping in FWI. This approach enables FWI to operate on transducers originally designed for B-mode imaging without requiring hardware modification. Our method provides a practical solution to overcome the cycle skipping encountered in FWI and improve sound speed reconstruction in ultrasound tomography.

REFERENCES

[1] Pedram, M. and Joe, L., "Ultrasound tomography for simultaneous reconstruction of acoustic density, attenuation, and compressibility profiles," *The Journal of the Acoustical Society of America* **137**(4), 1813–1825 (2015).

[2] Li, C., Duric, N., Littrup, P., and Huang, L., "In-vivo breast sound-speed imaging with ultrasound tomography," *Ultrasound in Medicine and Biology* **35**(10), 1615–1628 (2009).

[3] Wiskin, J., Borup, D., Johnson, S., and Berggren, M., "Non-linear inverse scattering: high resolution quantitative breast tissue tomography," *The Journal of the Acoustical Society of America* **131**(5), 3802–3813 (2012).

[4] Duric, N., Littrup, P., Poulo, L., Babkin, A., Pevzner, R., Holsapple, E., Rama, O., and Glide, C., "Detection of breast cancer with ultrasound tomography: First results with the computed ultrasound risk evaluation (CURE) prototype," *Medical physics* **34**(2), 773–785 (2007).

[5] Ali, R., Mitcham, T., and Duric, N., "Impact of starting model on waveform inversion in ultrasound tomography," in [*Medical Imaging 2023: Ultrasonic Imaging and Tomography*], **12470**, 89–98, SPIE (2023).

[6] Simon, B., Vadim, M., Dimitri, K., and Philippe, L., "Ultrasonic computed tomography based on full-waveform inversion for bone quantitative imaging," *Physics in Medicine & Biology* **62**(17), 7011–7035 (2017).

[7] Rehman, A., Trevor, M., Israel, O., Sarah, M., and Nebojsa, D., "Frequency-differencing strategy to kickstart full-waveform inversion without cycle skipping," *JASA Express Letter* **5**(1) (2025).

[8] Nuomin, Z., Yang, X., Yu, Y., Xudong, Y., and Yi, S., "Full-waveform inversion with low-frequency extrapolation based on sparse deconvolution for ultrasound computed tomography," *Ultrasound in medicine & biology* **51**(8), 1–15 (2025).

[9] Chen, Z., Cheng, D., Feng, W., and Wu, T., "An optimal 9-point finite difference scheme for the helmholtz equation with pml.," *International Journal of Numerical Analysis & Modeling* **10**(2) (2013).

[10] Rehman, A., Trevor, M. M., Thurston, B., Oscar, C. A., Cristina, D. M., Cuiping, L., Doyley, M. M., and Duric, N., "2-d slicewise waveform inversion of sound speed and acoustic attenuation for ring array ultrasound tomography based on a block lu solve," *IEEE Transactions on Medical Imaging* **43**(8), 2988–3000 (2024).

[11] Treeby, B. E. and Cox, B. T., "k-wave: Matlab toolbox for the simulation and reconstruction of photoacoustic wave fields," *Journal of biomedical optics* **15**(2), 021314 (2010).